manuscript no. falewicz˙aa˙1col˙ver˙b
April 5, 2009

Relationship between non-thermal electron energy spectra and *GOES* classes

R. Falewicz[1], P. Rudawy[1], and M. Siarkowski[2]

[1] Astronomical Institute, University of Wrocław, 51-622 Wrocław, ul. Kopernika 11, Poland
e-mail: falewicz@astro.uni.wroc.pl; rudawy@astro.uni.wroc.pl

[2] Space Research Centre, Polish Academy of Sciences, 51-622 Wrocław, ul. Kopernika 11, Poland
e-mail: ms@cbk.pan.wroc.pl

Received xx xx, 2008; accepted xx xx, 2009

ABSTRACT

Aims. We investigate the influence of the variations of energy spectrum of non-thermal electrons on the resulting *GOES* classes of solar flares.

Methods. Twelve observed flares with various soft to hard X-ray emission ratios were modeled using different non-thermal electron energy distributions. Initial values of the flare physical parameters including geometrical properties were estimated using observations.

Results. We found that, for a fixed total energy of non-thermal electrons in a flare, the resulting *GOES* class of the flare can be changed significantly by varying the spectral index and low energy cut-off of the non-thermal electron distribution. Thus, the *GOES* class of a flare depends not only on the total non-thermal electrons energy but also on the electron beam parameters. For example, we were able to convert a M2.7 class solar flare into a merely C1.4 class one and a B8.1 class event into a C2.6 class flare. The results of our work also suggest that the level of correlation between the cumulative time integral of HXR and SXR fluxes can depend on the considered HXR energy range.

Key words. Sun: chromosphere – Sun: corona – Sun: flares – Sun: magnetic fields – Sun: X-rays, gamma rays

1. Introduction

Despite recent progress, the source and acceleration mechanisms of particles in solar flares are still far from being understood. It is commonly accepted that, during the flare impulsive phase, non-thermal electron beams are accelerated in the solar corona and move along magnetic field lines to the chromosphere where they deposit their energy. Here, most non-thermal electrons lose their energy in Coulomb collisions while a tiny part of the electron energy is converted into hard X-rays (HXR) by bremsstrahlung. The heated chromospheric plasma evaporates and radiates over a wide spectral range from hard X-rays or gamma rays to radio emission. Hard and soft X-ray fluxes emitted by solar flares are generally related, in a way first described by Neupert (1968), who found

Send offprint requests to: R. Falewicz

that the time derivative of the soft X-ray flux approximately matches the microwave flux during the flare impulsive burst. A similar effect was also observed for hard X-ray emission (Dennis & Zarro (1993)). Since hard X-ray and microwave emissions are produced by non-thermal electrons and soft X-rays are the thermal emission of a hot plasma, the Neupert effect suggests that non-thermal electrons are the direct source of plasma heating. Lin et al. (1984) were the first to observe hard X-ray emission above 25 keV from microflares using balloon-borne observations. Later studies using RHESSI observations (Qiu et al. (2004); Battaglia et al. (2005); Hannah et al. (2008)) show that time, spatial and spectral characteristics of microflares are similar to those of large flares. However, there is no universal, unambiguous correlation between the released total energy of the flare and the observed HXR radiation.

Many flares reveal a low SXR emission (as indicated by GOES emission), but strong emission of the HXR emission above 30 keV (McDonald et al. (1999), Gburek & Siarkowski (2002), Qiu et al. (2004), Siarkowski et al. (2006)). Such events are commonly called "non-correlated" flares. Analytical estimations made by McDonald et al. (1999) show that in these flares, only a small part of the total energy carried by the non-thermal electrons is transferred to ambient material during the chromospheric evaporation process. Even so, analysis of the HXR emission of these flares allows one to estimate the energy flux of non-thermal electrons and to numerically simulate the energy losses and hydrodynamic effects of the chromospheric evaporation, thus allowing investigations of the energy budgets of the solar flares.

In this paper we investigate the influence of non-thermal electron energy distribution on the resulting *GOES* classes of flares and energy used by chromospheric evaporation. Our goal was to separate the influence the spectral index (δ) and low energy cut-off (E_c) of the non-thermal electron distribution, taken to be a power law in energy, from the total energy of the electrons. To do this we calculated a grid of 1D models to describe the time evolution of twelve observed solar flares. All the models of each observed flare were calculated using identical total energies delivered by non-thermal electrons but with various appropriate combinations of δ and E_c. For each model, we calculated the resulting *GOES* $1-8$ Å flux (i.e. *GOES* class of the event) as well as the evaporation energy.

In the following, we describe the observed flares (Section 2), the model calculation (section 3), the results obtained (Section 4) and the discussion and conclusions are given in Section 5.

2. Observations

We selected 12 disk flares observed by the *Yohkoh* satellite, having a simple single-loop X-ray structure and maximum hard X-ray flux not less than 10 ctns/sec per subcollimator of the M2 channel (33-53 keV) of the HXT instrument (Kosugi et al. (1991)). Details are given in Table 1. Five flares were analyzed by McDonald et al. (1999) (four being correlated and one non-correlated), a further seven flares were taken from the HXT Flare Catalogue (Sato et al. (2006)), four being correlated and three non-correlated. The correlated and non-correlated events are denoted in Table 1 with letters C and N respectively.

The flares were also observed with the *Yohkoh* SXT grazing-incidence telescope (Tsuneta et al. (1991)) and Bragg Crystal Spectrometer (*BCS*; Culhane et al. (1991)) as well as the *GOES* X-ray photometers (1-8 Å and 0.5-4 Å bands). HXT images of the flares were reconstructed using

Table 1. Physical parameters of observed flares.

Event date	Time of maximum [UT]	GOES class	GOES incremental class	Type of flare	γ	a_0 [ph/cm^2/sec/keV]	E_c [keV]	S [$10^{17} cm^2$]	L_0 [$10^8 cm$]
16-Dec-91	04:58	M2.8	M2.7	C	3.6	7.6×10^6	25.8	3.9	15.4
02-Feb-92	11:34	C5.5	C2.7	N	3.0	2.4×10^5	18.9	2.3	09.8
27-Oct-92	01:47	M1.1	C9.5	C	4.5	2.8×10^7	25.2	2.3	11.6
03-Oct-93	09:11	C1.0	B8.1	N	2.7	6.2×10^4	23.0	1.4	02.9
07-Mar-93	21:48	C1.5	B9.2	N	3.0	4.8×10^4	24.0	2.3	12.6
26-Jan-94	05:41	C1.4	C1.1	N	2.6	4.9×10^4	17.2	1.3	19.5
30-Jun-99	11:30	M1.9	M1.8	C	3.4	1.0×10^6	25.8	1.8	11.5
22-Dec-99	10:56	C6.4	C5.4	N	3.7	2.8×10^6	25.2	3.9	16.6
27-Jul-00	04:10	M2.5	M2.4	C	3.2	4.8×10^5	19.8	2.3	08.7
06-Apr-01	01:49	C7.8	C4.9	N	2.7	2.1×10^5	28.7	2.3	13.0
08-Sep-01	16:45	C5.1	C3.2	N	2.9	2.0×10^5	29.6	2.3	17.0
18-Sep-01	00:08	M1.5	M1.3	C	3.7	2.3×10^6	27.0	1.1	06.8

γ - photon spectral index; E_c - low energy cut-off; a_0 - scaling factor (flux at 1 keV);

S and L_0 - cross-section and semi-length of the flaring loop; Type of flare: C - correlated flare; N - non-correlated flare.

a standard Pixon method (Metcalf et al. (1996)) with variable accumulation times and an assumed threshold count rate of 200 counts in the M2 band (33-53 keV); these are shown in Figure 1. SXR images (also shown) of ten flares were taken with Be119/SXT, but for two flares, due to a lack of the SXT images, we present images taken with HXT in its L0 (14 - 23 keV) channel.

HXT spectra were analyzed to give the photon spectral index (γ) at the flare peak time in the M2 channel, flux scaling factor (flux at 1 keV = a_0) and cut-off energy in the electron distribution (E_c). The SXT images allowed us to estimate the single loop semi-length (L_0) and cross-section (S). These are given in Table 1.

3. Methods of analysis

Solar flare hard X-ray emission $\gtrsim$ 10-20 keV is generally believed to be produced by bremsstrahlung emitted by the non-thermal electrons. A power-law dependence of the emitted spectrum implies a power law energy distribution of the non-thermal electrons (Brown (1971); Tandberg-Hanssen & Emslie (1988)) and this in turn requires a low energy cut-off E_c of the electron spectrum to prevent an infinite total electron energy. A value of E_c has been arbitrary set by numerous authors between 15 and 25 keV (see e.g. McDonald et al. (1999) and references therein). Thus E_c is in the energy range where thermal emission can dominate and so it is very difficult to determine its correct value from observations.

With the improved spectral resolution of the *RHESSI* instrument, the thermal and non-thermal spectral components can be more clearly separated. Also, direct inversion of photon spectra is now possible to deduce the "mean electron flux distribution" (Brown et al. (2006)). But the problem of estimation E_c remains (e.g. Kontar et al. (2008)). In the absence of *RHESSI* data for these flares our approach has been to compare the *Yohkoh*/HXT observations of the 12 flares with results

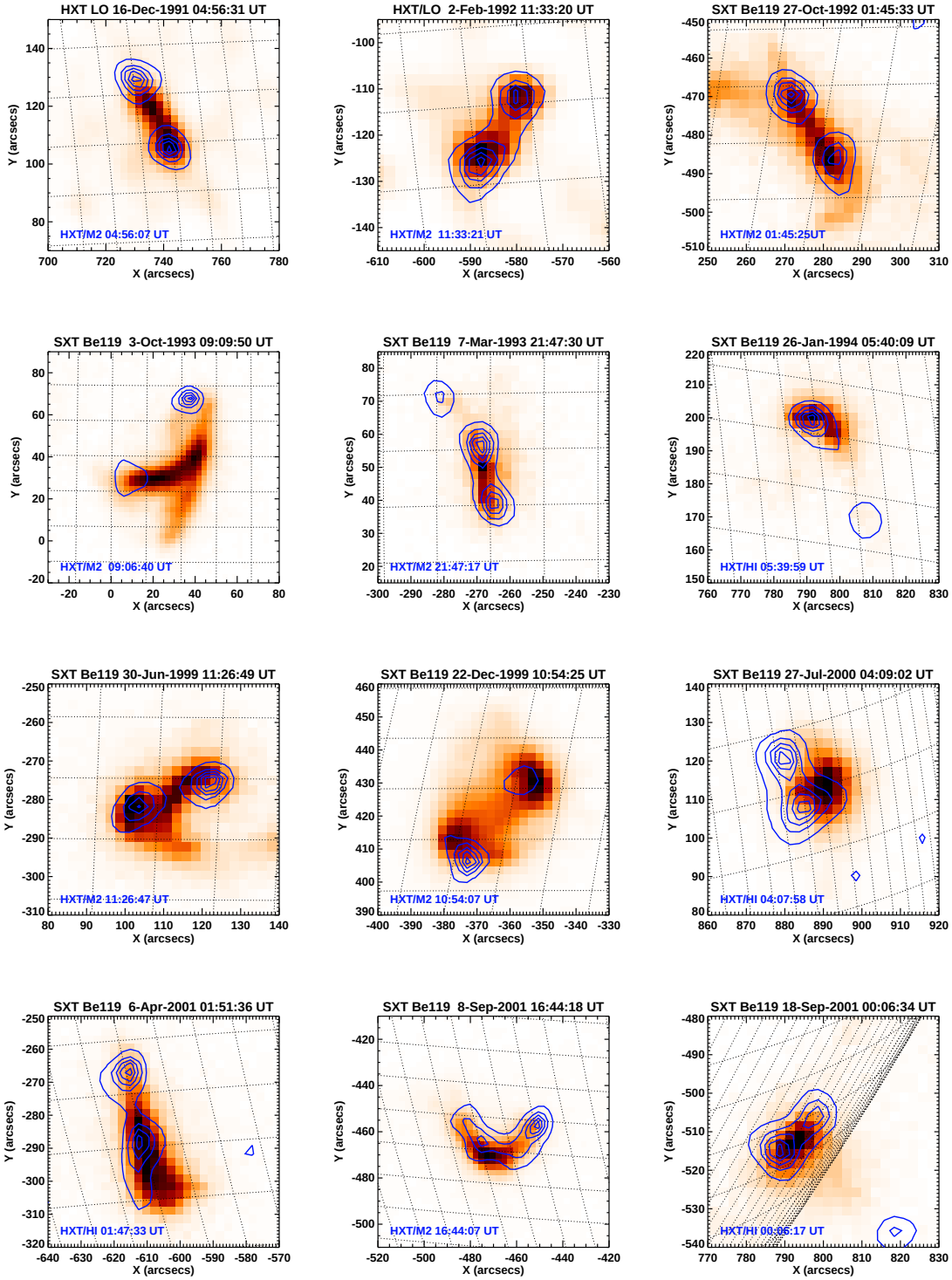

Fig. 1. Images of twelve analyzed flares taken with the *Yohkoh* SXT or HXT/LO (gray scale images) and HXT/M2 or HXT/HI (contours) instruments.

of model calculations. We investigated the relation between the non-thermal electron spectra and the *GOES* class of the thermal flare which is produced by evaporation processes using observed parameters of the 12 flares. Our calculations took into account the observed energy distributions of the non-thermal electrons and time variations of the observed X-ray fluxes, dimensions of the

flaring loops from SXR images, estimated main initial physical parameters of the thermal plasma (density, temperature), and energy gain and losses.

We analysed each flare in two steps: (a) we built a model of the observed flare that most closely resembled the synthesized and observed *GOES* and BCS light curves (when available); (b) we investigated how the variations of the non-thermal electron energy spectra influence the synthesized *GOES* fluxes of solar flare model.

The geometry of each flaring loop (volume (V), loop cross section (S) and half-length (L_0)) were determined using images taken with SXT and HXT (see Table 1). The loop cross sections were estimated as the areas within a level equal to 30% of the maximum flux in the HXT/M2 channel. Loop half lengths L_0 were estimated from the distances between the centres of gravity of the HXT/M2 footpoints, assuming a semi-circular shape for the loop. The volume of the loop V then equals $2\,L_0\,S$. Temperatures (T_e) and emission measures (EM) were estimated using *GOES* 1 - 8 Å and 0.5 - 4 Å fluxes using the filter-ratio method proposed by Thomas et al. (1985). We used here an updated version of this paper by White et al. (2005). A detailed description of this method is given also by Siarkowski et al. (2008). Mean electron densities (n_e) were estimated from emission measures (EM) and volumes ($V = 2L_0S$).

Assuming a power-law hard X-ray photon spectra $I(\epsilon) = a_0\epsilon^{-\gamma}$ we calculated time variations of the spectral indexes (γ) and scaling factors a_0 (flux at 1 keV) for the impulsive phases of all 12 flares. Electron spectra of the form of $F = A\,E^{-\delta}$ can be calculated from power-law photon spectra using thick target approximation (Tandberg-Hanssen & Emslie (1988)):

$$A = a_0\,\frac{4\pi R^2 C}{S\,\kappa_{BH}\bar{Z^2}}\,\frac{\gamma(\gamma-1)}{B(\gamma-1,\frac{1}{2})} \quad \text{and} \quad \delta = \gamma + 1 \tag{1}$$

where S is the loop cross-section area, R is the Earth-Sun distance (1 AU $\simeq 1.50\times10^{13}$ cm), κ_{BH} is the constant in the Bethe-Heitler cross-section (7.9×10^{-25}cm^2 keV), and $\bar{Z^2}$ is the abundance-weighted value of an atomic mass in the solar atmosphere, assumed to be equal to 1.4. The parameter C is defined as $2\pi e^4\Lambda \approx 2.6\times10^{-18}$ cm^{2}keV^2, where Λ is the Coulomb logarithm, and $B(x, y)$ is the complete beta function. The total energies radiated in the SXR range were calculated by summing energies emitted by the flaring loop in all time-steps of the model over the duration of the flare impulsive phase, using for each time-step the measured temperature (T_e), electron density (n_e) and corresponding emission function.

The estimated total energy carried by the non-thermal electrons is very sensitive to the assumed low-energy cut-off of the electron spectrum, E_c, due to the power-law nature of the energy distribution. A change of the E_c value by just a few keV can add or remove a substantial amount of energy from/to the modeled system, so E_c must be selected with great care. We estimated E_c as follows. First, we derived low energy cut-offs of the energy spectra using the slightly modified semi-analytical model of McDonald et al. (1999). While these authors used a fixed value of E_c (equal to 20 keV) for all flares, we calculated E_c for each flare using an iterative method. The flare energy budged was calculated using *GOES* and HXT data. When the total energies calculated from HXR data and those emitted in the SXR range disagrees, we iteratively changed the value of E_c (in steps of 0.1 keV) until agreement was achieved. This method is the most direct way to estimate E_c from the energy balance. We then slightly modified the value of E_c further in order to obtain the best agreement of the synthesised and observed *GOES* classes and BCS fluxes for each

flare. Examples of the agreement between observed and synthesised BCS light curves are shown in Figure 2 while the observed and synthesised *GOES* curves are shown in Figure 3. The estimated E_c was used as a fixed value while electron spectral index δ and corresponding scaling factor A varied in time for each particular model of event. The values of the main physical parameters, including γ and estimated E_c, observed at maximum of the HXR emission, are given in Table 1 for all twelve flares.

By changing the electron energy spectral index δ and appropriate adjustment of A and E_c, one can easily change the amount of the energy used for the evaporation process but keeping fixed the total energy flux delivered by non-thermal electrons**:**

$$\Phi = \int_{E_c}^{\infty} AE^{-\delta} E\, dE = \frac{A}{\delta - 2} E_c^{2-\delta} \tag{2}$$

For each time step during each flare and with values of δ and E_c chosen such that Φ is constant, one can calculate an appropriate value of A from (2). This allows one to generate a set of possible electron beams, all with identical total energy (integrated over the whole impulsive phase of the event) and identical time variations of the energy flux, and to use them to calculate a grid of models for each flare (see Fig. 4). For this work, we defined the impulsive phase of each flare as the period when the hard X-ray flux as recorded in HXT/M1 channel was larger than 10 percent of the maximum flux.

In this work we used a modified Naval Research Laboratory Solar Flux Tube Model code kindly made available to the solar community by Mariska and his co-workers (Mariska et al. (1982), Mariska et al. (1989)). Although a typical flaring loop is a 3-D structure surrounded by a possibly complex active region, it can be modeled for many purposes with a simple 1-D hydrodynamic model as with the NRL Code. We included a few modifications to the code: new radiative loss and heating functions; inclusion of the VAL-C model (Vernazza et al. (1981)) of the initial structure of the lower part of the loop (extended down using Solar Standard Model data (Bahcall & Pinsonneault (2004)); and use of double precision in the calculations. The heating of the plasma by a non-thermal electron beam was modeled using the approximation given by Fisher (1989). A mesh of new values of the radiative loss function was calculated using the CHIANTI (version 5.2) software (Dere et al. (1997), Landi et al. (2006)) in a temperature range $10^4 - 10^8$ K and density range $10^8 - 10^{14}$ cm^{-3}. For each flare a grid of models was calculated using various non-thermal electron beam models, all having the same total energy. All models were calculated for periods lasting from the beginning of the impulsive phase to beyond the soft X-ray emissions maximum. These periods were about 150-200 seconds. The time steps in the models were about 0.0005-0.001 sec.

We estimated the evaporation energy E_{evap} as the difference between the total energy delivered by the non-thermal electrons E_{nth} and the total energy lost by radiation over the whole loop, E_{rad} (i.e. $E_{evap} = E_{nth} - E_{rad}$) over the impulsive phase. As mentioned before, the main parameters of each calculated model (time-dependent fluxes of the non-thermal electrons and the lengths and cross-sections of the flaring loops) were evaluated using observational data (see Section 2).

4. Results

We analysed each flare in two steps. First, we built a model using observed geometrical and physical parameters, including δ and E_c. The correctness of these models was validated by comparison of

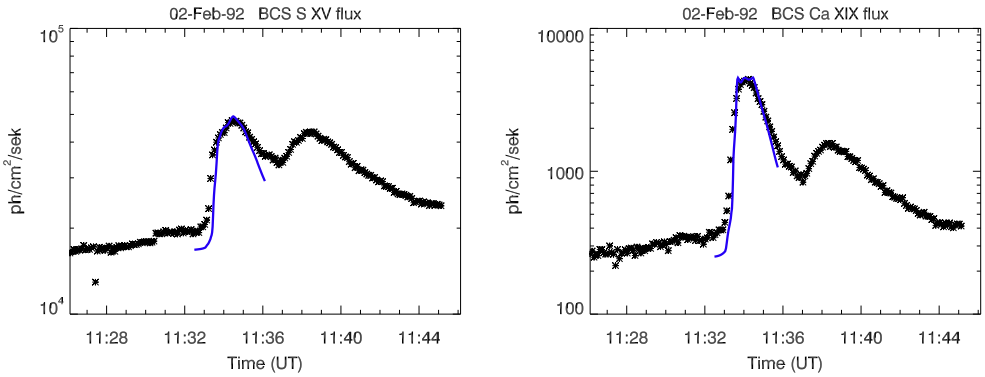

Fig. 2. Synthesised BCS CaXIX and BCS SXV fluxes (blue lines), and the observed fluxes (asterisks) of the C2.7 class solar flare observed on 1992 February 2.

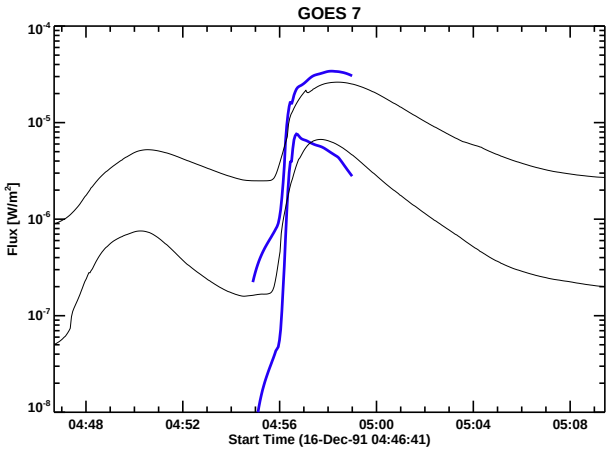

Fig. 3. Synthetic X-ray fluxes in 0.5-4 Å and 1-8 Å bands calculated using a numerical model of the M2.7 class solar flare observed on 1991 December 16 (blue thick line) and the corresponding fluxes recorded with the *GOES* 7 satellite (thin grey lines).

the synthesized *GOES* 1-8 Å and 0.5-4 Å, BCS SXV and BCS CaXIX fluxes with the observed fluxes. We achieved good agreement between observations and the modeled data. For example, the observed and synthesized BCS SXV and BCS CaXIX fluxes of the C2.7 class solar flare observed on 1992 February 2 are shown in Figure 2 while the calculated and observed *GOES* X-ray light-curves of the M2.7 event on 1991 December 16 are shown in Figure 3. The values of the flux maxima are reproduced very well but the large discrepancies noticeable during the early rise and late decay phases are caused by lack of an additional pre- and post-impulsive flare heating in our model. In the second step, we calculated several numerical models of each event for various appropriate combinations of the electron spectral index δ and low-energy cut-off E_c, keeping fixed the total energy delivered by the non-thermal electrons equal to the observed energy.

The model calculations also provide pressure, temperature, density, velocity, column mass etc. as function of time and position along the loop. For all reasonable sets of physical parameters of the flaring loops we found a fast inflow of chromospheric material into the loop (i.e. chromospheric evaporation). Large-scale macroscopic motions of the dense plasma toward the loop-tops and fast increases of the plasma temperature, pressure, electron density all agree well with commonly accepted schemes of chromospheric evaporation. After the energy deposition period, the plasma contained in the flaring loop gradually cools but the model calculations generally ended before returning to a hydrostatic equilibrium.

Table 2. Results of the numerical models of analysed flares

Event date	OBSERVATIONS GOES class*	MODEL Minimum GOES class*	E_{evap}/E_{nth}	MODEL Maximum GOES class*	E_{evap}/E_{nth}
16-Dec-91	M2.8 (M2.7)	C2.4 (C1.4)	0.07	M9.5 (M9.4)	0.79
02-Feb-92	C5.5 (C2.7)	C3.4 (B6.3)	0.17	C8.4 (C5.6)	0.78
27-Oct-92	M1.1 (C9.5)	C2.5 (B9.5)	0.08	M1.8 (M1.6)	0.82
03-Oct-93	C1.0 (B8.1)	B6.5 (B4.4)	0.19	C2.8 (C2.6)	0.71
07-Mar-93	C1.5 (B9.2)	B9.5 (B3.7)	0.07	C2.4 (C1.8)	0.70
26-Jan-94	C1.4 (C1.1)	B7.4 (B4.4)	0.22	C2.8 (C2.5)	0.84
30-Jun-99	M1.9 (M1.8)	C2.0 (B9.9)	0.04	X1.1 (X1.1)	0.71
22-Dec-99	C6.4 (C5.4)	C2.1 (C1.1)	0.06	M4.5 (M4.4)	0.66
27-Jul-00	M2.4 (M2.3)	C4.2 (C3.2)	0.11	M4.7 (M4.6)	0.80
06-Apr-01	C7.8 (C4.9)	C4.5 (C1.5)	0.07	M3.1 (M2.8)	0.68
08-Sep-01	C5.1 (C3.2)	C1.9 (A2.4)	0.02	M1.4 (M1.2)	0.51
18-Sep-01	M1.5 (M1.3)	C3.1 (C1.1)	0.05	M4.8 (M4.6)	0.72

**GOES* class minus the preflare level is given in parentheses.

For all twelve flares we found that keeping total energy delivered by non-thermal electrons fixed, the resulting observed *GOES* class of the induced solar flare varied significantly when the spectral index and low energy cut-off of the non-thermal electrons spectra were changed. The variations of the *GOES* classes and the proportion of the total energy contributed by evaporation are given in Figure 4. The upper left panel shows models of M2.7 *GOES* class correlated flare observed on 1991 December 16. The observed low energy cut-off E_c is equal to 25.8 keV and is assumed constant during the calculations. The spectral index δ is equal to 4.6 (here and for the other three events shown on Figure 4 we give the value of δ at the time of maximum of the impulsive phase). The upper right panel shows models of the C2.7 *GOES* class non-correlated flare observed on 1992 February 2. The observed E_c and δ are equal to 18.9 keV and 4.0. The lower left panel shows models of the B8.1 *GOES* class non-correlated flare observed on 1993 October 3. Observed E_c and δ are equal to 23 keV and 3.7. Bottom right panel shows models of the M2.4 *GOES* class correlated flare observed on 2000 July 27. Observed E_c and δ are equal to 19.8 keV and 4.2. The spectral indexes δ of each model varied in time in accordance with its observational values increased or decreased by a constant factor. In other words, in our models, we took various values of δ that were different than δ_{obs} by amounts from 0 up to ±2, where δ_{obs} is the observed δ at any given time during the flare. The black, filled squares represent models calculated using non-thermal electron beams having main parameters deduced from observations. The total ranges of the modeled *GOES* classes and E_{evap} for all flares are shown in Table 2.

We now describe results obtained for the most representative events, two correlated flares (1991 December 16, 2000 July 27) and two non-correlated flares (1992 February 2 and 1993 October 3). All flares had a simple, single-loop structure. (In the following GOES classes are given with the pre-flare level subtracted.)

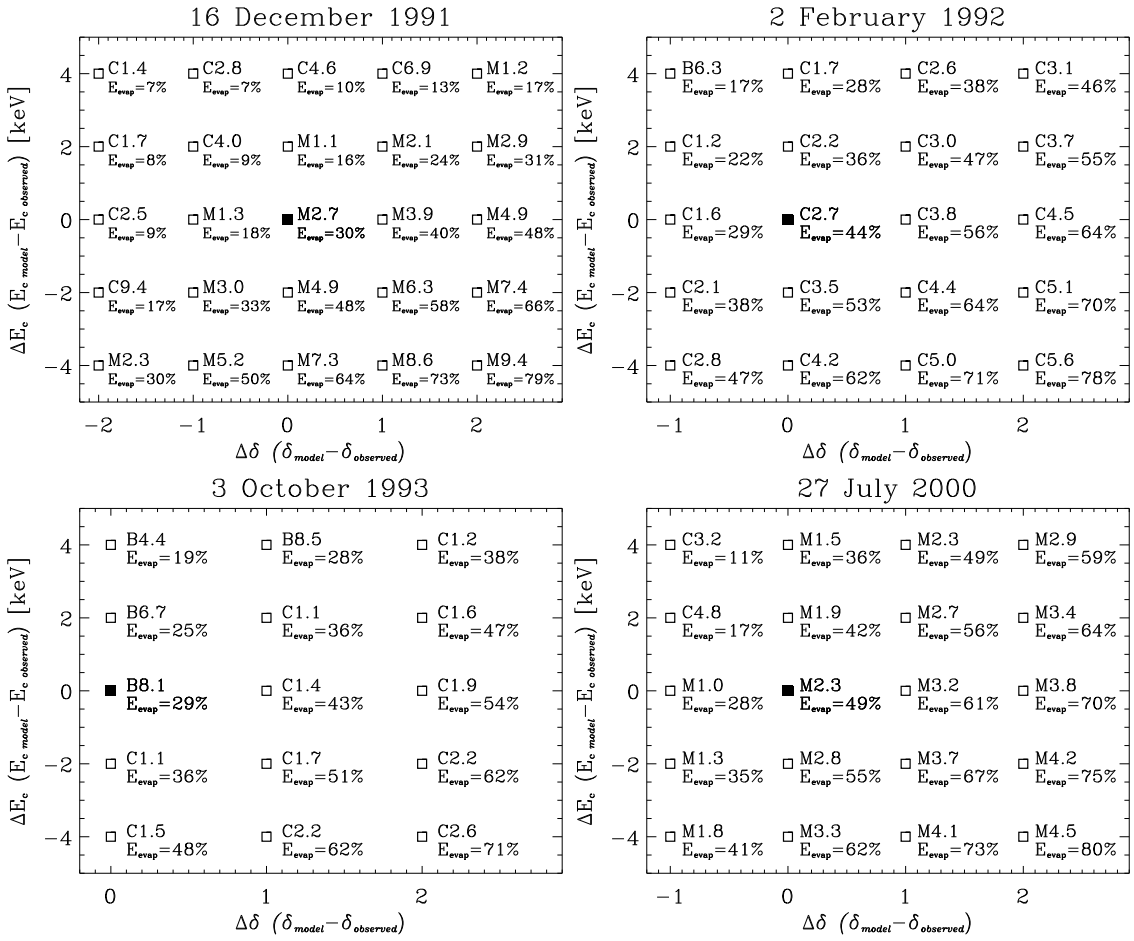

Fig. 4. Variations of the observed *GOES* classes and shares of the evaporation energy E_{evap} in the total energies delivered by non-thermal electrons for four solar flares observed on 1991 December 16, 1992 February 2, 1993 October 3 and on 2000 July 27. See Section 4 for details.

4.1. M2.7 flare on 1991 December 16

The M2.7 flare at 04:54 UT on 1991 December 16 occurred in active region NOAA 6961 (N04W45). The flare appeared in SXR as a single loop with semi-length 15 400 km (see Fig. 1). The impulsive HXR (>23 keV) occurred between 04:55:50 UT and 04:56:28 UT. The cross-section of the loop was estimated from HXR images to be $S = 3.9 \times 10^{17}$ cm^2.

A flare model was calculated using parameters of the photon spectra γ and scaling factors a_0 calculated as a function of time from hard X-ray fluxes observed in the HXT $M1$ and $M2$ channels, while E_c was estimated and fixed as equal to 25.8 keV. The total non-thermal electron energy estimate to be $E_{nth} = 1.2 \times 10^{30}$ ergs while the evaporation energy was $E_{evap} = 3.6 \times 10^{29}$ ergs (= $0.3\,E_{nth}$). Alternative models were calculated for the same total energy E_{nth} but with δ changed from the initial value of 4.6 by ±2 and with E_c changed from the initial value of E_c by ±4 keV (see Figure 4, top left panel). For δ lowered by 2 and E_c raised by 4 keV the evaporation energy decreased to 7% of the E_{nth} only while the *GOES* class decreased to only C1.4. By contrast, for δ increased by 2 and E_c lowered by 4 keV the observed *GOES* class of the event increased to M9.4 while the evaporation energy increased to 79% of E_{nth}. Calculations made for all combinations of δ and E_c give flares of with *GOES* class varying between C1.4 and M9.4.

4.2. C2.7 flare on 1992 February 2

The C2.7 flare on 1992 February 2 at 11:33 UT - 11:38 UT occurred in active region NOAA 7042 (S14W41). It was observed with HXT/*Yohkoh* and *GOES* only (see Fig. 1). The impulsive HXR (>23 keV) peak occurred between 11:33:18 UT and 11:33:28 UT, only 10 s long. HXT/LO images of the flare show the X-ray emission as a single loop with semi-length ($\simeq$ 9800 km). The loop foot points were observed in HXT channels M2 and H only. The loop cross-section was estimated as $S = 2.3 \times 10^{17}$ cm^2.

The flare model was calculated as for the previous flare. The total energy was $E_{nth} = 1.7 \times 10^{29}$ ergs and the evaporation energy was $E_{evap} = 7.5 \times 10^{28}$ ergs, ($= 0.44 E_{nth}$). Alternative models were calculated for the same total non-thermal electron energy E_{nth} but with δ in the range -1 to +2 from the initial value of δ and with E_c in the range ±4 keV from the initial value of E_c (see Figure 4, top right panel). Calculations made for all combinations of spectral index and low energy cut-off give flares of *GOES* classes in range B6.3 and C5.6.

4.3. B8.0 flare on 1993 October 3

The B8.1 flare on 1993 October 3 occurred between 09:06 UT and 09:07 UT in active region NOAA 7590 (N11W04). The flare was visible in SXT as a single loop of semi-length ~ 28 800 km (see Fig. 1). The impulsive HXR (>23 keV) emission occurred between 09:06:40 UT and 09:07:15 UT. The cross-section of the loop was estimated as $S = 1.4 \times 10^{17}$ cm^2.

A flare model was calculated using the total energy equal to $E_{nth} = 1.6 \times 10^{29}$ ergs. The evaporation energy was equal to $E_{evap} = 4.6 \times 10^{28}$ ergs, ($= 0.29 E_{nth}$). Alternative models were calculated for the same total energy E_{nth} but with δ changed by 0 to +2 from the initial value of δ and with E_c changed from the initial value of E_c by ±4 keV (see Figure 4, bottom left panel). For the spectral index increased by 2 and energy cut-off lowered by 2 keV the evaporation energy of the flare increased to 0.71 E_{nth} and the *GOES* class of the flare increased to C2.6. Calculations made for all combinations of spectral index and energy cut-off give flares of *GOES* classes varying from B4.4 to C2.6.

4.4. M2.4 flare on 2000 July 27

The M2.4 flare on 200 July 27 occurred between 04:08 UT - 04:13 UT in active region NOAA 9090 (N10W72). The flare was visible in SXT as a single loop with semi-length ~ 8700 km (see Fig. 1). The HXR (>23 keV) emission occurred between 04:07:54 UT and 04:08:30 UT. Using the reconstructed HXR images we estimated the cross-section of the loop to be $S = 2.3 \times 10^{17}$ cm^2.

The flare model was calculated in the same way as for the previous events. The total energy was equal to $E_{nth} = 4.8 \times 10^{29}$ ergs and the evaporation energy $E_{evap} = 2.3 \times 10^{29}$ ergs ($= 0.44 E_{nth}$). The alternative models of the flare were calculated for the same total energy E_{nth} but with δ changed from the initial value of δ by -1 to -2 and with E_c changed from the initial value of E_c by ±4 keV (see Figure 4, bottom right panel). For the spectral index increased by 2 and energy cut-off lowered by 4 keV the evaporation energy of the flare increased to 80% of the E_{nth} and the *GOES* class of the flare increased to M4.5. By contrast, for δ lowered by 1 and E_c raised by 4 keV the observed *GOES* class of the event lowered to only C3.2 while the evaporation energy decreased to 0.11 E_{nth}.

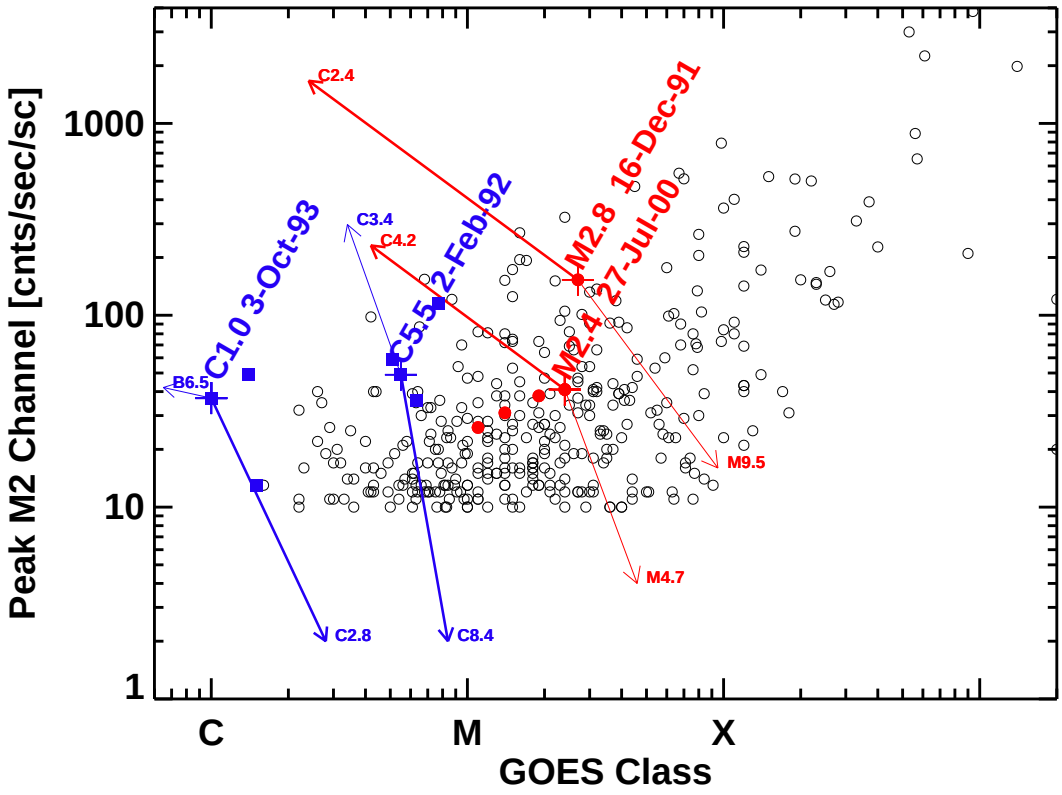

Fig. 5. Variations of the synthesised *GOES* classes and X-ray fluxes of the numerical models of the four solar flares obtained for various E_c and δ and constant total energy delivered by non-thermal electrons (see main text and Fig. 4 for details). The models calculated using observed energy spectra of non-thermal electrons are marked with crosses. The arrows show the variations of the *GOES* classes and X-ray fluxes of the models, the open circles represent 369 flares taken from the Sato HXT Flare Catalogue. Filled circles (red colour) denote five correlated and filled squares (blue colour) seven non-correlated analysed flares.

Calculations made for all combinations of δ and E_c give flares with *GOES* classes varying from C3.2 to M4.6.

5. Discussion and conclusions

We have presented results of an energy model calculation for twelve flares having various soft to hard X-ray emission ratios. Our interest was focused on the influence of the variations of the energy spectrum of the non-thermal electrons on the resulting observed *GOES* classes of the flares and on their evaporation energies E_{evap}. Many numerical models of the events were calculated using observed and modified energy distributions of the non-thermal electrons (various appropriate combinations of the electron spectral index δ and low energy cut-off E_c but fixed value of the total energy delivered by non-thermal electrons E_{nth}), observed geometry of the loops and initial values of the main physical parameters of the plasma estimated using observational data. We showed first that with fixed initial parameters of the flare loop (geometry and physical parameters of the plasma) as well as fixed total non-thermal electron energy, one can significantly change the resulting *GOES* class of the flare by appropriate change of the electron index and low energy cut-off of the electron spectra while maintaining the total energy at a constant value. For example, we were able to change

the M2.7 *GOES* class correlated flare into only a C1.4 class non-correlated-like flare and the B8.1 *GOES* class non-correlated flare into a C2.6 class correlated-like flare.

The ratio of the radiated energy to the energy in evaporation processes as well as observed *GOES* classes of the events vary for various combinations of the spectral index and low energy cut-off. It is obvious that both the total delivered energy and the energy spectrum of the non-thermal electron beam (described by spectral index and low energy cut-off) are decisive for the course and magnitude of the evaporation processes as well as for determination of the observed soft X-ray emission of the flares (i.e. their *GOES* class).

An estimation of the energy carried by non-thermal electrons is very sensitive to an assumed value of the low energy cut-off of the energy spectrum due to the power law nature of the energy distribution. A change of the E_c value by only a few keV can add or remove a substantial amount of energy from/to the modeled system. The spectral index of the non-thermal electron spectrum is also crucial, while the low-energy fraction of the electrons heats the chromospheres most effectively (see also McDonald et al., 1999). For the same total energy the beam of non-thermal electrons with a softer spectrum could give rise to a solar flare of greater *GOES* importance. This is demonstrated in Figure 4, where variations of the observed *GOES* classes and evaporation energies E_{evap} are shown for four flares. As an example one can track the behaviour of the M2.7 flare on 1991 December 16. The model calculated using a non-thermal electron beam having main parameters deduced from observations, the *GOES* class is equal to M2.7 and the evaporation energy equals 30% of the total energy delivered by the non-thermal electrons. The same observed solar flare, modeled using non-thermal electron beam having spectral index δ decreased by 1, has a slightly lower *GOES* class equal to M1.3 and significantly lower evaporation energy equal to 18% E_{nth}. By increasing additionally the low energy cut-off E_c by 2 keV we obtained an even lower *GOES* class and E_{evap} of the model equal to C4.0 and 9% E_{nth}, respectively. By contrast, for a steeper electron spectrum and increased population of the low energy electrons (decreased E_c), the *GOES* classes and E_{evap} increase. Thus, for the M2.7 flare described above, the non-thermal electron beam with energy spectral index δ increased by 1 has a slightly higher *GOES* class equal to M3.9 and higher evaporation energy equal to 40% E_{nth}. By decreasing additionally the low energy cut-off E_c by 2 keV (expanding the low-energy electrons' population) we obtained even higher *GOES* class and E_{evap} of the model equal to M6.3 and 58%, respectively. The ranges of the modeled *GOES* classes and E_{evap} for all analysed events are given in Table 2.

The overall course of changes of *GOES* classes and E_{evap} is similar for all our analysed events. In general, the SXR emission increases for softer HXR spectra and decreases for harder spectra. That is, the steeper electron spectra result in a higher amount of evaporated material. Such behaviour is induced by spatial variations of an efficiency of the non-thermal electrons' energy deposition mechanism. The energy deposition mechanism is most efficient in the transition region and upper part of the chromosphere, but its particular spatial distribution depends on a actual distribution of the column mass of plasma encountered by non-thermal electrons. However, the magnitude of changes observed for a particular flare depends on the flare's physical proprieties.

A non-thermal electron beam having a large population of high-energy electrons (i.e. having a hard spectrum) penetrates deep into the chromospheric plasma where it deposits most of its energy, from where energy is efficiently radiated. The remaining part of the carried energy is deposited in the upper part of the chromosphere and/or transition region, causing moderate "gentle evaporation".

On the other hand, a non-thermal electron beam having soft spectrum deposits most of its energy in the upper part of the chromosphere and/or transition region, where the density is relatively low, giving rise to ”explosive evaporation”.

Our results show that the parameters and properties of the solar flares depend not only on the initial hydrodynamic properties of the flaring loop and on the total amount of the delivered energy but also on properties of the primary source of energy and time and spatial variations of the processes leading to the acceleration of the electrons. Thus, the level of correlation between the cumulative time integral of HXR and SXR fluxes depends on the HXR energy range. Such a conclusion is in accordance with results of the statistical analysis of flares by Veronig et al. (2002) and microflares by Qiu et. al. (2004) observed with RHESSI indicating that only half of the events show a time behaviour consistent with the expectations based on the Neupert effect. Qiu et al. (2004) showed also that the correlation resulting from the Neupert effect is greatest in the photon energy range of 14-20 keV.

In Figure 5 we show variations of the synthesised *GOES* classes and X-ray fluxes of the numerical models of the four solar flares obtained for various E_c and δ and constant total energy delivered by non-thermal electrons. The arrows show the variations of the *GOES* classes and X-ray fluxes of the models while the open circles represent 369 flares taken from the HXT Flare Catalogue (Sato et al. (2006)). As can be seen the relationships between soft and hard X-ray fluxes obtained from the models go far beyond the range of the ”correlation belt” of soft and hard X-ray fluxes recorded for the observed solar flares, up to high HXR fluxes. For example, by changing the hardness of the non-thermal electron spectrum and low energy cut-off the M2.7 flare observed on 1991 December 16 was converted into the C2.4 *GOES* class event having an HXT/M2 peak emission above 1000 cnts/sec/sc (see Figure 5, thick arrow). Many flares with low GOES class but with large hard X-ray flux have been observed with *Yohkoh* and *RHESSI*. However, one does not observe flares with similar GOES class having very large X-ray flux; the Nature apparently do not realise extremely ”small-hard” flares (i.e. those which would be located in the upper-left corner at the Figure 5). This than imposes restrictions on the flare electron spectra and therefore on acceleration mechanisms.

Acknowledgements. The authors would like to thank the *Yohkoh* team for excellent solar data and software. They are also grateful to the anonymous referee for useful comments and suggestions.

This work was supported by the Polish Ministry of Science and Higher Education, grant number N203 022 31/2991 and by the European Community’s Seventh Framework Programme (FP7/2007-2013) under grant agreement n° 218816 (SOTERIA).

References

Bahcall, J. N., & Pinsonneault, H. M. 2004, Phys. Rev. Lett., 92, 12

Battaglia, M., Grigis, P. C., & Benz, A. O. 2005, A&A, 439,737

Brown, J. C. 1971, Solar Phys., 18, 489

Brown J. C., Emslie, A. G., Holman, G. D., et al. 2006, ApJ, 643, 523

Culhane, J. L., Bentley, R. D., Hiei, E., et al. 1991, Solar Phys., 136, 89

Dennis, B. R., & Zarro, D. M. 1993, Solar Phys., 146, 177

Dere, K.P., Landi, E., Mason, H.E., Monsignori-Fossi, B.C., & Young, P.R. 1997, A&AS, 125, 149

Gburek, S., & Siarkowski, M. 2002, Adv. Space Res., 30/3, 601

Hannah, I. G., Christe, S., Krucker, S., et al. 2008, ApJ, 677, 704

Fisher, G. H. 1989, ApJ, 346, 1019

Kontar, E. P., Dickson, E., & Kaparov, J. 2008, Solar Phys. 252, 139

Kosugi, T., Masuda, S., Makishima, K., et al. 1991, Solar Phys., 136, 17

Lin, R. P., Schwartz, R. A., Kane, S. R., et al. 1984, ApJ, 283, 421

Landi, E., Del Zanna, G.,Young, P.R., et al. 2006, ApJS, 162, 261

Mariska, J. T., Boris, J. P., Oran, E. S., Young, T. R. Jr., & Doschek, G. A. 1982, ApJ, 255, 738

Mariska, J. T., Emslie, A. G., & Li, P. 1989, ApJ, 341, 1067

McDonald, L., Harra-Murnion, L. K., & Culhane, J. L. 1999, Sol. Phys., 185, 323

Metcalf, T. R., Hudson, H. S., Kosugi, T., Puetter, R. C., & Pina, R. K. 1996, ApJ, 466, 585

Neupert, W. M. 1986, ApJ, 153, L59

Qiu, J., Liu, C., Gary, D.E., Nita, G.M., & Wang, H. 2004, ApJ, 612, 530

Sato, J., Matsumoto, Y., Yoshimura, K., Kubo, S., et al. 2006, Solar Phys., 236, 351

Siarkowski, M., Falewicz R., & Berlicki A. 2006, Adv. Space Res., 38/5, 972

Siarkowski, M., Falewicz, R., Kepa, A., & Rudawy, P. 2008, Ann. Geophys., 26, 2999

Tandberg-Hanssen, E., & Emslie, A. G. 1988, *The physics of solar flares*, Cambridge University Press

Thomas, R. J., Crannell, C. J., & Starr, R. 1985, Solar Phys., 95, 323

Tsuneta, S., Acton, L., Bruner, M., et al. 1991, Solar Phys., 136, 37

Vernazza, J., Avrett, E., & Loeser, R. 1981, ApJS, 45, 635

Veronig, A., Vrsnak, B., Dennis, B. R., et al. 2002, A&A, 392, 699

White, S., Thomas, R. J., & Schwartz, R. A. 2005, Sol. Phys., 227,231